How to cite: *Angew. Chem. Int. Ed.* **2021**, *60*, 18217–18222
International Edition: doi.org/10.1002/anie.202105468
German Edition: doi.org/10.1002/ange.202105468

Single-Molecule Studies

The Influence of a Changing Local Environment during Photoinduced CO_2 Dissociation

*Michael Vyshnepolsky, Zhao-Bin Ding, Prashant Srivastava, Patrik Tesarik, Hussain Mazhar, Matteo Maestri, and Karina Morgenstern**

Abstract: *Though largely influencing the efficiency of a reaction, the molecular-scale details of the local environment of the reactants are experimentally inaccessible hindering an in-depth understanding of a catalyst's reactivity, a prerequisite to maximizing its efficiency. We introduce a method to follow individual molecules and their largely changing environment during a photochemical reaction. The method is illustrated for a rate-limiting step in a photolytic reaction, the dissociation of CO_2 on two catalytically relevant surfaces, Ag(100) and Cu(111). We reveal with a single-molecule resolution how the reactant's surroundings evolve with progressing laser illumination and with it their propensity for dissociation. Counteracting processes lead to a volcano-like reactivity. Our unprecedented local view during a photoinduced reaction opens the avenue for understanding the influence of the products on reaction yields on the nanoscale.*

Introduction

The underlying physical principles of reactions on metallic surfaces are accessible through ultra-short laser illumination.[1–4] Photolytic chemistry on metallic surfaces induces reactions at low temperatures, where thermal reactions are completely suppressed. If the photon energy is not in resonance with the adsorbate, the reactions are initiated by the absorption of the laser light by the electrons of a metallic sample, which then either heat the sample or directly attach to an adsorbate to induce reactions.[5] So far, mostly desorbing particles were analyzed, giving ensemble information.[5,6] On the other hand, a seminal scanning tunneling microscopy (STM) study revealed that a catalyst undergoes severe restructuring in course of a reaction.[7] We demonstrate here the importance of a local view during a photoinduced reaction for the archetypical CO_2 dissociation, an important and generic example for a rate-limiting process in a catalytic reaction.[8,9] It is, for instance, the first step in the reverse water-gas shift reaction, which is widely used on copper-based catalysts for the conversion of CO_2 to produce liquid fuels.[10–12] On the other hand, the (100) surface of Ag nanoparticles was shown to dominate in electrochemical environments.[13] Besides, CO_2 has gained widespread interest because of its contribution to the greenhouse effect, making CO_2 dissociation through reduction a primary goal.[14] Coupling a femtosecond laser to an STM,[15,16] we unravel three steps in the dissociation process on Ag(100) and Cu(111) at advancing illumination through resolving the surroundings of specific reactants in real space. Our unprecedented local information about the reactivity of individual molecules in a specific environment on a photoinduced chemical reaction opens the avenue for a microscopic understanding of the influence of the environment on reactivity.

Results and Discussion

CO_2 molecules, imaged as protrusions on the quadratic Ag(100) face, form variably-shaped multi-domain clusters (Figure 1a).[17] To identify the progression during the CO_2 dissociation, such a sample is alternately illuminated and imaged (Figure 1b–d), for laser parameters and other details see the Supporting Information, Experimental Section. The unique setup[18] allows us to image exactly the same region of the surface before and after illumination.

In the example shown in Figure 1, similar laser power and thus absorbed peak fluence (i.e. energy per area and pulse at the maximum of the Gaussian-shaped laser pulse) is used for the first 8×10^6 pulses. The first two million pulses, at a peak fluence of ca. 9 $\mu J\,cm^{-2}$ per pulse lead to a change in the shape of the clusters and a slight reduction in their size (Figure 1b). These changes are considerably more substantial after the next two million pulses, even at a comparable peak fluence of 12 $\mu J\,cm^{-2}$ per pulse (Figure 1c). Besides, novel features appear on the terraces between the original CO_2 clusters, simple depressions, and depressions with a protrusion in their center (circles in Figure 1c). Comparison to earlier work identifies these as CO molecules[19] and oxygen atoms,[20] respectively, implying photoinduced CO_2 dissociation. Apparent depressions within the CO_2 clusters (one marked by an

[*] Dr. M. Vyshnepolsky, P. Srivastava, P. Tesarik, H. Mazhar, Prof. Dr. K. Morgenstern
Physikalische Chemie I, Ruhr-Universität Bochum
Universitätsstraße 150, 44801 Bochum (Germany)
E-mail: karina.morgenstern@rub.de
Dr. Z.-B. Ding, Prof. Dr. M. Maestri
Laboratory of Catalysis and Catalytic Processes,
Dipartimento di Energia, Politecnico di Milano
via La Masa 34, 20156 Milano (Italy)
Supporting information and the ORCID identification number(s) for the author(s) of this article can be found under: https://doi.org/10.1002/anie.202105468.

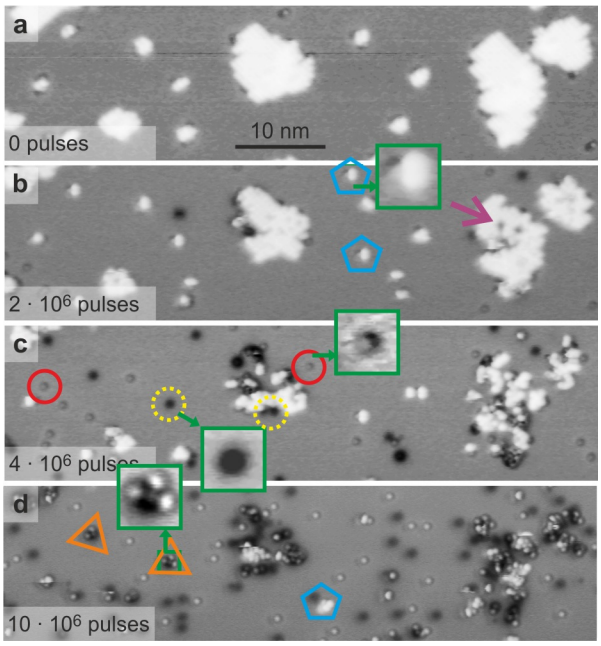

Figure 1. Progressing dissociation of CO_2 on Ag(100): a)–d) selected images with total number of pulses with respect to (a) leading to accumulated peak fluences of (b) 18.3 J cm^{-2} (c) 43.6 J cm^{-2} (additional accumulated peak fluence between b and c: 25.3 J cm^{-2}) (d) 127.1 J cm^{-2} (d). Markers: red circles: CO molecules; yellow dashed circles: oxygen atoms; cyan pentagons: agglomerations of CO_2 at CO; orange triangles: agglomerations of CO at O; one structure each is enlarged for better visibility by a factor of 3 and shown at enhanced contrast in the green squares, purple arrow in (b) points to an apparent depression within a CO_2 cluster; 6.5 pA, 100 mV.

arrow in Figure 1 b) suggest that some of the oxygen atoms remain close to the reactants.

After 10^7 pulses, very few CO_2 molecules remain (Figure 1 d). Larger black regions at the positions of the original CO_2 clusters confirm that the majority of the oxygen atoms remain close to their place of dissociation. As a side reaction, CO_2 molecules are expelled from larger clusters, forming novel smaller clusters on the terrace close to products from previous reactions (marked by pentagons in Figure 1 b,d). These might be the origin of some of the oxygen atoms far away from the original CO_2 clusters. In contrast, the other product, CO, is more evenly distributed pointing to an additional photoinduced process, a molecular motion. Thereby, it is conceivable that the excess energy released upon dissociation is transformed into translational energy or that subsequent laser pulses induce a motion of the dissociated species. A minor diffusivity of the CO during subsequent laser illuminations implies that a substantial excess energy of the dissociation leads to their motion across the surface. Note that some of the CO molecules are adsorbed so close to the oxygen atoms that they are likely to be trapped in their vicinity yet at a distance too large for direct interaction (agglomerates, marked by triangle Figure 1 d). Most notably, the number of reactions seems not to be proportional to the number of illuminations.

This impression is confirmed for molecularly resolved CO_2 clusters (Figure 2). Despite the larger statistical uncertainty, we present here the analysis of a single cluster for quantification, because a local dependence of the processes makes the same effect being operative at slightly different illumination times for different clusters. Initially, the cluster

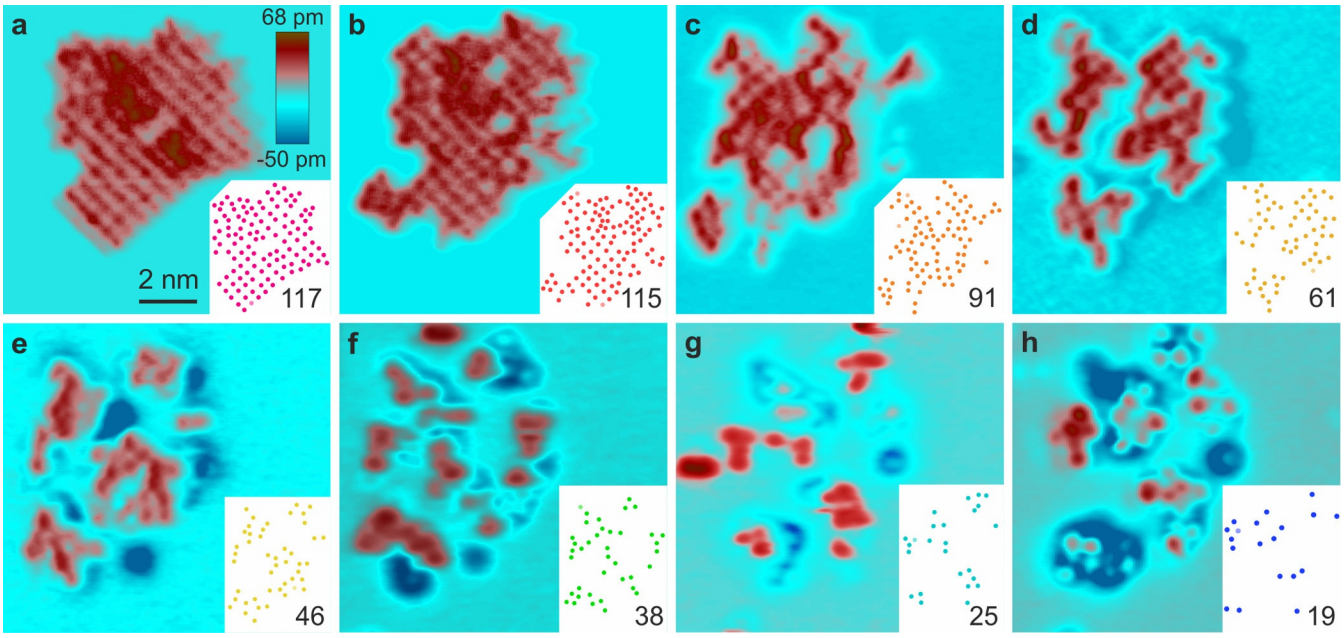

Figure 2. Progressing dissociation of an individual CO_2 cluster on Ag(100): a to h) STM images on a false-color scale; insets: one dot per CO_2 molecule within the corresponding cluster with the number of molecules; 6 pA, 250 mV; a to f) single illuminations of 10^6 pulses leading to an accumulated peak fluence of 55.5 J cm^{-2}, that is, average peak fluence per pulse: 11.1 μJ cm^{-2} (f to g) 3×10^6 pulses at a peak fluence per pulse of 10.8 μJ cm^{-2} for an accumulated peak fluence of 78.7 J cm^{-2} (g to h) 2×10^6 pulses at a peak fluence per pulse of 19.6 μJ cm^{-2} leading to an accumulated peak fluence of 127.2 J cm^{-2} between (a) and (h).

consists of 117 CO_2 molecules mostly in quadratic symmetry (Figure 2a). The first illumination with 10^6 pulses reduces the total number of CO_2 molecules only slightly to 115. However, the order of the cluster, especially at its top right, is largely reduced (Figure 2b). The next train of 10^6 pulses increases the disorder and reduces the number of CO_2 molecules within the cluster significantly to 91 (Figure 2c). The largest absolute change by a third to 61 molecules is induced during the next train of 10^6 pulses (Figure 2d). The original cluster is split into three smaller ones. Quadratic symmetry is no longer recognizable after the next train of 10^6 pulses, reducing the number of molecules to 46 (Figure 2e). The number of molecules continues to decrease, but comparatively little for the next 3×10^6 pulses, with only 5 molecules per 10^6 pulses (Figure 2f). We thus increase the fluence per pulse for the final 2×10^6 pulses (Figure 2g to h). The small changes between Figures 2f and h emphasize that the dissociation yield is largely reduced.

To quantify these changes demands a precise alignment of the STM tip to the maximum of the Gaussian-shaped laser spot. This is achieved with the aid of two-photon photoelectrons generated by the laser in the metal and collected by the tip, for details see Experimental Methods in the Supporting Information. The dissociation yield is quantified at the peak position as $Y_{i\rightarrow i+1}=\Delta N/(N_{\mathrm{phot}}N_i)$, a yield that is normalized to the number N_i of CO_2 molecules available for dissociation in illumination number i. $\Delta N=N_i-N_{i+1}$ is the number of dissociated CO_2 molecules and N_{phot} the number of absorbed photons per adsorbed molecule. Because of a slight variation in laser power for the different trains of laser pulses and a larger single-pulse fluence for the last illuminations, we display the dissociation yield versus the peak fluence F_{acc} accumulated over all pulses since the beginning of the measurement. This is a valid procedure because the process is linear in the number of photons (see the Supporting Information).

The quantum yield varies by more than one order of magnitude between less than 10^{-7} and more than 10^{-6} dissociated molecules per absorbed photon and adsorbed molecule for the cluster in Figure 2 (Figure 3a, left axis). It is almost negligible for the first illumination. After a steep increase, the yield decreases monotonously, reaching again an almost negligible value at an accumulated peak fluence of 127 J cm^{-2}, despite the availability of further CO_2 molecules. As the yield is normalized to the number of undissociated molecules, this decrease cannot be explained simply by the reduced availability of reactants. Instead, such a volcano-like shape of the yield points to two counteracting processes, one that increases and another one that decreases the yield.

The qualitative discussion above suggests that the geometry of the clusters influences the yield (for further details see supplementary material). To quantify the geometrical changes to the clusters, we display a shape value $S=16A/P^2$, with A the island area and P its perimeter length (Figure 3a, right axis). This ratio equals 1 for a perfectly quadratic cluster and reduces for less compact structures. The shape value decreases rapidly up to an accumulated peak fluence of ca. 40 J cm^{-2}, reflecting the decrease in compactness of the cluster (cf. Figure 2e). Then, the shape value stays, at (0.11 ± 0.02), almost constant, corresponding to a cluster

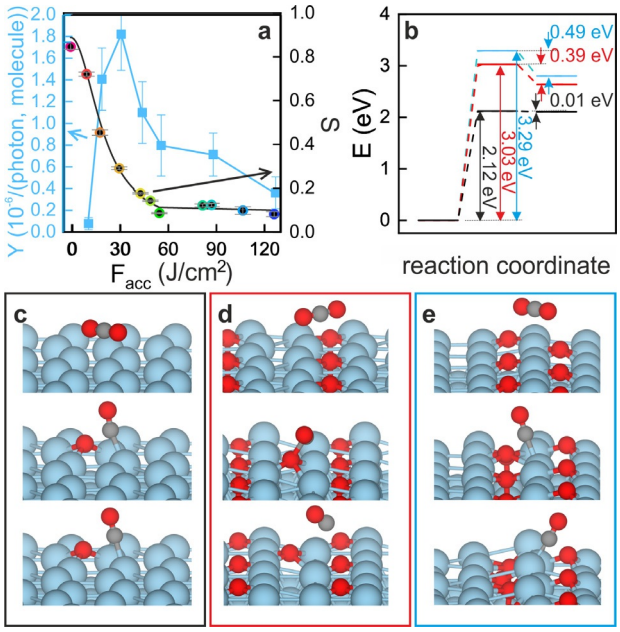

Figure 3. Fluence-dependent dissociation yield with modeling: a) left axis: Dissociation yield Y per available molecule and absorbed photon (squares); right axis: shape value $S=16A/P^2$ (dots) of cluster shown in Figure 2 versus accumulated peak fluence F_{acc}; connecting lines and fit to guide the eye. b) Calculated thermal dissociation barriers for CO_2 dissociation on a pristine surface (black), a surface precovered with 0.25 ML oxygen (red), and a surface precovered with 0.33 ML oxygen (blue) as depicted in (c to e) with initial (top), transition (middle), and final state (bottom).

whose perimeter is around three times longer than for a quadratic cluster of the same size. The increase in yield at decreasing shape value (Figure 3a) implies that dissociation is more likely for molecules in a non-ordered than in an ordered cluster, possibly due to faster dissipation of the excitation energy within an ordered cluster, which instead causes its rearrangement. Thus, cooperative effects reduce the dissociation yield. On the other hand, the environment of the CO_2 cluster is increasingly altered with progressing dissociation by products in the vicinity of the clusters (Figure 1b to d). Their emergence correlates with a reduction in yield. It suggests that self-poisoning is the counteracting process that reduces the dissociation yield.

To understand this self-poisoning, we first explore how the small number of absorbed photons available at 10 μJ cm^{-2} peak fluence per pulse, achieves the photoinduced dissociation. For a laser illumination that is not in resonance with the adsorbate levels, the electrons of the metal absorb the photon energy.[5] A transfer of the electron energy to the lattice could heat it transiently to temperatures that are sufficient to induce a reaction thermally. However, for the low peak fluences per pulse in the range of μJ cm^{-2} employed here, the maximum temperature on Ag(100) does not surpass 10 K, as estimated by the two-temperature model.[21] More efficiently, the resulting energetic electrons transfer their energy directly to an adsorbate to activate it. Their reaction yield is governed by the density of excited carriers in the energy interval of the adsorbate resonance. As a non-thermal electron distribution

persists on the picosecond time scale for μJ cm^{-2} fluences per pulse,[22] for example, 1 ps in Cu,[23] non-thermalized electrons are expected to attach to the adsorbates to initiate their reaction. Thereby, the electron density is not sufficient for multiple excitations at the low fluences used here because of the small number of absorbed photons per molecule,[24] here ca. 0.2 photons per pulse and adsorbed molecule. This implies that a single electron needs to carry sufficient energy for dissociation, that is, the process is linear in fluence. This reasoning is supported by the same results achieved in an experiment performed at a longer pulse length (see supporting information).

The maximum energy of electrons directly after excitation corresponds to the photon energy, here 3.1 eV. Poisoning could thus result from a dissociation barrier that is increased above this value. Since the influence of CO on the surface charge is considerably weaker than that of oxygen,[25] we explore the influence of coadsorbed oxygen atoms on the thermal dissociation barrier to corroborate this reasoning. The calculation of the thermal barriers yields a reasonable estimate of the energy barrier as the relaxation of the electron from the adsorbate to the metal happens on a faster timescale (<1 ps) than the nuclear motion leading to dissociation (>1 ps),[5] such that the dissociation itself is expected to evolve on the same (or a rather similar) potential energy landscape as thermal dissociation. Because the vibrationally excited molecules could also dissociate following other than the energetically most favorable pathway, the thermal barrier represents the lowest energy pathway that might lead to dissociation.[5]

To explore the influence of oxygen on the thermal barrier, we calculated direct CO_2 dissociation reactions on three surfaces: a pristine Ag(100) surface, one that is covered by oxygen in 0.25 ML coverage, and one that is covered in 0.33 ML coverage. The CO_2 molecules are found to be physisorbed on all surfaces (Figure 3c to e). All initial and final states are defined as the global minima at both sides of the transition states, which are already similar to the configurations of the final states, where CO and O are dissociated. The dissociation barrier increases from 2.13 eV on the clean surface to 3.03 eV and further to 3.29 eV in the presence of 0.25 ML and 0.33 ML bystander O, respectively (Figure 3b). This is in line with the fact that the barrier of CO_2 dissociation becomes larger for less oxophylic conditions. The increases in dissociation barriers can be understood in terms of a late transition state for the dissociation, for which the barrier is more affected by the final state. Because of repulsion, the binding energy of the CO product is reduced in the presence of oxygen and consequently, the barrier for CO_2 dissociation moves upwards. This reduces the dissociation yield to negligible values, as observed experimentally.

Having revealed the reason for self-poisoning, we demonstrate that the two counteracting processes are not restricted to one material or symmetry by performing a similar experiment on Cu(111), for which theory predicts a similar increase in thermal dissociation barrier for oxygen dissociation.[9] For Cu(111) the activation barriers for CO_2 dissociation increased from 1.48 eV to 3.25 eV, that is, above the energy of a single photon, already at 0.2 ML oxygen.[9]

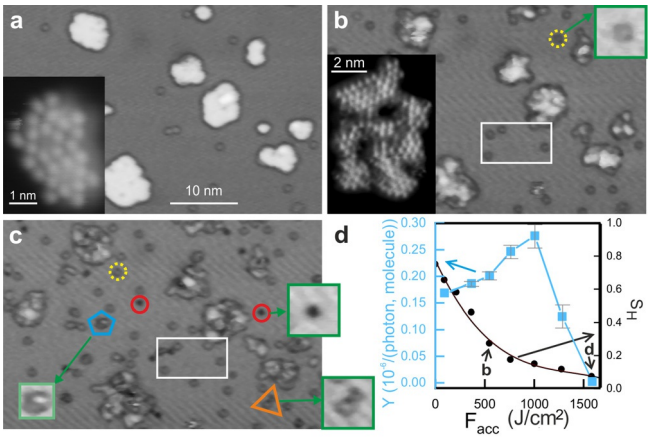

Figure 4. Progressing dissociation of CO_2 on Cu(111): a to c) selected images with 4×10^6 laser pulses each between the panels leading to accumulated peak fluences of (b) 518 J cm^{-2}, that is, ca. 130 μJ cm^{-2} on average per pulse (c) 1555 J cm^{-2} (additional peak fluence between b and c: 1037 J cm^{-2}, that is, ca. 260 μJ cm^{-2} on average per pulse); 6 pA, 250 mV. Markers: red circles: CO molecules; yellow dashed circles: oxygen atoms; cyan pentagon: agglomeration of CO_2 at CO; orange triangle: agglomeration of CO at O; one structure each is enlarged by a factor of 2 and shown at enhanced contrast in the green squares; white rectangles to point out negligible photoinduced diffusivity of the products (a) 9 pA, 50 mV (b) 10 pA, 100 mV. (d) Dissociation yield Y per available molecule and absorbed photon (squares, left axis) and shape value $S_H = 24/\sqrt{3}A/P^2$, (dots, right axis) of individual island versus accumulated peak fluence F_{acc}; connecting lines and fit to guide the eye.

On Cu(111), the CO_2 molecules form multi-domain hexagonal clusters (Figure 4a).[17] Despite the difference in both, crystal material and face, the results of laser illumination are largely identical (Figure 4a to c). As on Ag(100), a change in cluster shape is accompanied by a loss in order (compare molecular resolution in the insets in Figure 4a,b), which is reflected in the shape value $S_H = 24/\sqrt{3}A/P^2$, here defined such that a perfect hexagon gives $S_H = 1$ to account for the different cluster symmetry (Figure 4d). Again, two novel species (marked by circles in Figure 4c) and agglomerates of CO close to oxygen (one marked by a triangle) are formed on the terrace, small amounts of CO_2 are transported from clusters to products (one CO_2-CO agglomerate marked by a pentagon), and the clusters split into smaller ones.

The photoinduced mobility of the reactants is even smaller on Cu(111) than on Ag(100) (e.g. rectangle in Figure 4b,c), reflecting a lower thermal diffusion barrier of CO molecules on Ag(100) (72 meV[26]) than on Cu(111) (98 meV[9]). Thus, also on Cu(111), the large-scale transport of particles away from the CO_2 clusters is related to the excess energy of the reaction.

The CO_2 dissociation yield Y per molecule is here defined as $Y_{i\rightarrow i+1} = \Delta A/\Delta F A_i$ with the area A_i (apparent height above 45 pm) representing CO_2 molecules available in illumination i and the change in area due to a loss of CO_2 molecules $\Delta A = A_i - A_{i+1}$. The yield first increases, as on Ag(100), (Figure 4d, left axis). The maximum of the yield is followed by a steep decrease to an almost negligible value during the final illumination, besides the availability of further non-dissoci-

ated CO_2 molecules. As compared to Ag(100), the yield starts at a higher value and increases more gradually. This is in line with an initially more disordered cluster and a less prominent change in shape S_H (Figure 4d, right axis). The differences between Ag(100) and Cu(111) in the increase of the yield are thus related to a structural mismatch of the adsorbate with the surface (cf. Ref. [17]) and not to the electronic structure of the metal.

The two surfaces differ further in the accumulated peak fluence necessary to achieve similar effects. It is more than an order of magnitude higher on Cu(111) than on Ag(100). This is surprising as copper is a more efficient catalyst than silver in thermal reactions as reflected in the thermal dissociation barriers presented above and in Ref. [9]. The lower yield is thus related to processes that are only relevant to a photo-induced reaction. These are a) the number of electrons available for excitation and b) the electronic excitation and deexcitation mechanisms of the molecules. Considering already the absorbed fluence, the number of electrons could be reduced in the case of Cu(111) by a faster electron–phonon coupling and by a faster diffusivity of the electrons into the bulk. While the heat conductivities differ by only 10% in favor of silver, the electron-phonon coupling for copper is roughly 2.2-fold the one of silver.[27,28] As the dissociation is linear in the number of absorbed photons (see the Supporting Information), the largely reduced reaction rate results only partly from the faster transport of the electrons into the bulk. Thus, either electron coupling to the adsorbate is less active or the electron lifetime on it is much shorter on Cu(111) than on Ag(100). The lower diffusivity of all molecules on Cu(111) than on Ag(100), discussed above, points to a stronger adsorption of the reactants on Cu(111) in favor of a shorter electron lifetime on the adsorbate as the reason for the reduced reaction yield. None of these processes is expected to influence the specific shape of the yield curve, which results from the two counteracting processes of disordering and poisoning.

Conclusion

The gained local view on surface poisoning lines out how to unravel local effects in photoinduced reactions. While the surface poisoning should happen at similar energy independent of the type of light source, the local investigation on the length scale of molecules and its quantification to resolve underlying dynamics demands the precision of a laser experiment. The local investigation of intermediate states during a photochemical reaction, as first presented here, is potentially rich. It should result in a better microscopic understanding of the influence of the specific changes in the environment of the reactants on photochemical as well as thermal reactions.

Acknowledgements

We acknowledge financial support from the German Science Foundation (DFG) through grant MO 960/25-1 and under Germany's Excellence Strategy—EXC-2033—project number 390677874 RESOLV. Open access funding enabled and organized by Projekt DEAL.

Conflict of Interest

The authors declare no conflict of interest.

Keywords: density functional theory · poisoning · scanning tunneling microscopy · single-molecule studies

[1] A. H. Zewail, *Angew. Chem. Int. Ed.* **2000**, *39*, 2586 – 2631; *Angew. Chem.* **2000**, *112*, 2688 – 2738.
[2] H. Petek, M. J. Weida, H. Nagano, S. Ogawa, *Science* **2000**, *288*, 1402 – 1404.
[3] H. Öström, H. Öberg, H. Xin, J. LaRue, M. Beye, M. Dell'Angela, J. Gladh, M. L. Ng, J. A. Sellberg, S. Kaya, et al., *Science* **2015**, *347*, 978 – 982.
[4] B. Wezisla, J. Lindner, U. Das, A. C. Filippou, P. Vöhringer, *Angew. Chem. Int. Ed.* **2017**, *56*, 6901 – 6905; *Angew. Chem.* **2017**, *129*, 7005 – 7009.
[5] C. Frischkorn, M. Wolf, *Chem. Rev.* **2006**, *106*, 4207 – 4233.
[6] a) R. Frigge, T. Hoger, B. Siemer, H. Witte, M. Silies, H. Zacharias, T. Olsen, J. Shiotz, *Phys. Rev. Lett.* **2010**, *104*, 256102; b) G. Füchsel, J. C. Tremblay, T. Klamroth, P. Saalfrank, C. Frischkorn, *Phys. Rev. Lett.* **2012**, *109*, 33098303.
[7] T. Zambelli, J. Wintterlin, J. Trost, G. Ertl, *Science* **1996**, *273*, 1688.
[8] a) U. Burghaus, *Prog. Surf. Sci.* **2014**, *89*, 161 – 217; b) A. E. Green, J. Justen, W. Schöllkopf, A. S. Gentleman, A. Fielicke, S. R. Mackenzie, *Angew. Chem. Int. Ed.* **2018**, *57*, 14822 – 14826; *Angew. Chem.* **2018**, *130*, 15038 – 15042.
[9] L. Dietz, S. Piccinin, M. Maestri, *J. Phys. Chem. C* **2015**, *119*, 4959 – 4966.
[10] J. Ma, N. Sun, X. Zhang, N. Zhao, F. Xiao, W. Wei, Y. Sun, *J. Phys. Chem. Lett.* **2010**, *1*, 3053 – 3057.
[11] C. Liu, et al., *J. Am. Chem. Soc.* **2015**, *137*, 8676 – 8679.
[12] Y. A. Daza, J. N. Kuhn, *RSC Adv.* **2016**, *6*, 49675 – 49691.
[13] S. Liu, B. Yang, E. Tyo, S. Seifert, J. DeBartolo, B. von Issendorf, P. Zapol, S. Vajda, L. A. Curtiss, *J. Am. Chem. Soc.* **2017**, *139*, 2160 – 2163.
[14] Z. Wang, H. Song, H. Liu, J. Ye, *Angew. Chem. Int. Ed.* **2020**, *59*, 8016 – 8035; *Angew. Chem.* **2020**, *132*, 8092 – 8111.
[15] L. Bartels, F. Wang, D. Möller, E. Knoesel, T. F. Heinz, *Science* **2004**, *305*, 648 – 651.
[16] C. Zaum, K. M. Meyer-auf-der-Heide, M. Mehlhorn, S. McDonough, W. F. Schneider, K. Morgenstern, *Phys. Rev. Lett.* **2015**, *114*, 146104.
[17] M. Vyshnepolsky, K. Morgenstern, *Phys. Chem. Chem. Phys.* **2020**, *22*, 497 – 506.
[18] M. Mehlhorn, H. Gawronski, L. Nedelmann, K. Morgenstern, *Rev. Sci. Instrum.* **2007**, *78*, 033905.
[19] C. Zaum, K. Morgenstern, *Phys. Rev. Lett.* **2018**, *121*, 185901.
[20] S. Schintke, S. Messerli, K. Morgenstern, J. Nieminen, W.-D. Schneider, *J. Chem. Phys.* **2001**, *114*, 4206 – 4209.
[21] a) S. I. Anisimov, B. L. Kapeliovich, T. L. Perel'man, *Sov. Phys. JETP* **1974**, *39*, 375 – 377; b) R. Darkins, D. Duffy, University College London, private communication.
[22] R. H. M. Groeneveld, R. Sprik, A. Lagendijk, *Phys. Rev. B* **1995**, *51*, 11433 – 11445.
[23] W. S. Fann, R. Storz, H. W. K. Tom, J. Bokor, *Phys. Rev. B* **1992**, *46*, 13592 – 13595.
[24] J. W. Gadzuk, *Chem. Phys.* **2000**, *251*, 87 – 97.

[25] B. W. J. Chen, D. Kirvassilis, Y. Bai, M. Mavrikakis, *J. Phys. Chem.* **2019**, *123*, 7551 – 7566.
[26] B. Eren, R. S. Weatherup, N. Liakakos, G. A. Somorjai, M. Salmeron, *J. Am. Chem. Soc.* **2016**, *138*, 8207 – 8211.
[27] Z. Lin, L. V. Zhigilei, *Phys. Rev. B* **2008**, *77*, 075133.
[28] S. Babar, J. H. Weaver, *Appl. Opt.* **2015**, *54*, 477 – 481.

Manuscript received: April 21, 2021
Accepted manuscript online: May 17, 2021
Version of record online: July 9, 2021

